Two-photon imaging of capillary blood flow in olfactory bulb glomeruli

Emmanuelle Chaigneau, Martin Oheim, Etienne Audinat, and Serge Charpak*

Laboratory of Neurophysiology, Institut National de la Santé et de la Recherche Médicale EPI 0002, Centre National de la Recherche Scientifique FRE2500, Ecole Supérieure de Physique et Chimie Industrielles de la Ville de Paris, 10 Rue Vauquelin, 75231 Paris, France

Edited by Marcus E. Raichle, Washington University School of Medicine, St. Louis, MO, and approved August 25, 2003 (received for review June 13, 2003)

Analysis of the spatiotemporal coupling between neuronal activity and cerebral blood flow requires the precise measurement of the dynamics of RBC flow in individual capillaries that irrigate activated neurons. Here, we use two-photon microscopy *in vivo* to image individual RBCs in glomerular capillaries in the rat dorsal olfactory bulb. We find that odor stimulation evokes capillary vascular responses that are odorant- and glomerulus-specific. These responses consist of increases as well as decreases in RBC flow, both resulting from independent changes in RBC velocity or linear density. Finally, measuring RBC flow with micrometer spatial resolution and millisecond temporal resolution, we demonstrate that, in olfactory bulb superficial layers, capillary vascular responses precisely outline regions of synaptic activation.

Noninvasive imaging techniques have been widely used to determine the distributions of brain regions activated by sensory stimulations. Although several techniques detect contrast changes based on activity-dependent hemodynamic changes, the precise coupling between neuronal activation, energy demand, and changes in blood flow remains unclear (for review, see refs. 1–3). Analysis of the coupling requires a simultaneous measurement of the activity of neurons and the dynamics of local blood flow. Recently, measurements of extracellular activity combined with functional MRI (fMRI) have shown that field potential amplitude (4) and spiking frequency (5) are related to blood oxygen level-dependent (BOLD) signals (6, 7). These observations are a technical *tour de force*; yet, the spatial and temporal resolutions of fMRI are not sufficient to provide a precise understanding of the entire chain of cellular and vascular events elicited by the stimulation. In the cerebellar cortex, recent "semiinvasive" techniques requiring a craniotomy and using electrophysiological recordings combined with laser Doppler flowmetry have allowed more precise investigations and have demonstrated that the relationship between presynaptic and postsynaptic activity with blood flow varies according to the activated input (8–11). However, these studies did not measure blood flow in the individual capillaries that precisely irrigate the activated neurons, a prerequisite to analyzing the neurovascular coupling in detail.

Two-photon microscopy imaging of blood flow represents an alternative approach to studying this coupling (12) *in vivo*. It allows measurements of RBC flow with micrometer spatial resolution and millisecond temporal resolution in individual capillaries and can be combined with electrophysiological recordings (13, 14). If performed in a brain region where synaptic interactions are topographically organized, two-photon imaging should allow measurements of vascular flow in a given capillary irrigating a small population of neurons and glial cells. Because of its anatomical and functional organization, the rodent main olfactory bulb (15) is particularly suitable for such a study: all sensory cells expressing a given odorant receptor type send their axons to the bulb, where they converge onto only a few topographically fixed glomeruli (16, 17). Thus, all nasal sensory cells are represented by less than ≈2,000 glomeruli. As a result, odor stimulation reproducibly activates small glomeruli ensembles. These patterns of glomerular activation have been revealed by several methods including (*i*) BOLD fMRI (18–20), (*ii*) optical imaging of calcium (21), voltage (22), and intrinsic signals (23–28), (*iii*) electrophysiological recordings (29–31), and (*iv*) measurements of 2-deoxyglucose consumption (32, 33). Here, we use two-photon imaging to determine with a high spatial resolution the relationship between RBC flow in individual capillaries and neuronal activation. We find that odor evoked changes in capillary RBC flow that are odor- and glomerular-specific and exclusively limited to the zone of synaptic interactions, and that RBC velocity and RBC linear density are two independent variables.

Methods

***In Vivo* Electrophysiology and Odor Stimulations.** Wistar rats, postnatal days 30–60, were anesthetized with 1.5 g/kg urethane i.p. and held in a standard stereotaxic apparatus with ear bars. A craniotomy was performed above the two olfactory bulb hemispheres. In some experiments, the posterior cisterna was drained and the dura was removed. In other experiments, both imaging and recording were performed through the dura. Because no difference was found between these two paradigms, data were pooled. To record field potential, a borosilicate micropipette was filled with 2 M NaCl and 0.004% Oregon green dextran (molecular weight 10,000) and then placed under visual control by using two-photon imaging in a single glomerulus that was previously labeled (see below). A 100-μm-thick glass coverslip was placed over the bulb and fixed on the cranium, and the space below was filled with a 3% agar solution. Electrophysiological signals recorded with a Neuro Data amplifier (Cygnus Technology, Delaware Water Gap, PA) were digitized and stored on a PC (Digidata 1200A, Clampex 8, Axon Instruments, Foster City, CA). In addition, electrophysiological data were simultaneously acquired and synchronized to the images. Odors (isoamyl acetate, almond, and propionic acid) were applied for a duration of 2 sec with a custom-built olfactometer. The temperature of the animal was monitored with a rectal thermometer and maintained at 37°C with a feedback-controlled heating blanket (Harvard Apparatus). Teflon tubing was used from the odor reservoir to the nose. In about half of the cases, a drop of blood was taken from the femoral artery several times during the experiment to ensure that PO_2, PCO_2, and pH values and electrolyte content were normal [means: PO_2 = 93 ± 6 mmHg (1 mmHg = 133 Pa), PCO_2 = 36 ± 7 mmHg, saturation = 96.9 ± 0.5%; pH = 7.37 ± 0.03]. Samples were immediately analyzed by using a Rapidlab 348 analyzer (Bayer, Wuppertal, Germany).

***In Vivo* Two-Photon Imaging.** Axon terminals from the olfactory nerve (and thus glomeruli) were labeled with Oregon green

This paper was submitted directly (Track II) to the PNAS office.

Abbreviations: BOLD, blood oxygen level-dependent; fMRI, functional MRI; GL, glomerular layer; ONL, olfactory nerve layer.

See commentary on page 12535.

*To whom correspondence should be addressed. E-mail: serge.charpak@espci.fr.

dextran (molecular weight 10,000) by using the methods developed by Wachowiak and Cohen (21), 2–5 days before recording RBC flow. To label vessels, a bolus of 70-kDa fluorescein dextran (2.5–20 mg) was injected i.v. through a catheter placed in the femoral vein. Fluorescein dextran and Oregon green dextran were excited and imaged by using a custom two-photon laser-scanning microscope (14). An 830-nm excitation beam from a femtosecond Ti:Sapphire laser (5-W pump; Coherent Radiation, Palo Alto, CA) was focused into olfactory nerve terminals and capillaries by using a ×63 Leica (Deerfield, IL) water-immersion objective. Galvanometric scanners (Cambridge Technology, Cambridge, MA) controlled by home-built electronics and software (LABVIEW) were used to produce repetitive single-line scans at ≈2,000 lines per sec or images from subregions of the field of view at rates up to 20 frames per sec.

RBC Flow Analysis. Images acquired with longitudinal line scans were binarized, allowing detection of individual RBCs and measurements of RBC flow, velocity, linear density, and longitudinal size. In each binarized image, two lines were then drawn (yellow dotted lines in Fig. 2*B*) near the beginning and the end of the capillary length scanned by the laser. Two binary functions of time were obtained to determine the arrival time of each RBC at the two loci, and cross-correlations between the two series were then used to calculate the velocity for each RBC. Linear density was calculated as the ratio of flow/velocity. Mean values of flow, velocity, and linear density were calculated by averaging instantaneous values over 15–30 sec of acquisition. The power density spectra were calculated for RBC flow, velocity, and linear density after resampling at 1 kHz. Average values are expressed as mean ± SEM. The significance of changes in RBC flow, velocity, and linear density was assessed by comparing the mean values calculated over two 2-sec intervals, before odor stimulation and during the maximum of the effect.

Measuring Vessel Diameters. To measure capillary diameters, we acquired *Z*-stacks of images encompassing entirely the vessels. We then projected each stack onto a two-dimensional image and measured the internal diameter of the vessel by counting the fluorescent pixels.

Results

Location of Capillaries in the Rat Dorsal Olfactory Bulb. In the dorsal olfactory bulb, blood vessels were heterogeneously distributed. Large arteries and veins running along the surface were first identified according to their color under white light. After i.v. injection of fluorescein dextran, these vessels were then followed in depth by using two-photon imaging. In the first 100 μm, veins divided into numerous branches, whereas arteries hardly branched. As a result, this first ≈100-μm layer contained mainly veins and venules. We observed arterio-arterial, veno-venous, and arterio-venous anastomosis. Vessels were considered capillaries when their inner diameter was ≤6 μm. Capillaries were absent from the surface until a depth of ≈100–150 μm; on average, they appeared 138 ± 14 μm from the surface (mean ± SEM, $n = 31$ animals).

To precisely analyze the vascular architecture in the olfactory bulb superficial layers, we labeled glomeruli by intranasal injections of Oregon green dextran 2–5 days before microcirculation experiments. Subsequent two-photon imaging revealed fluorescent axons and terminals and allowed us (*i*) to separate the olfactory nerve layer (ONL) from the glomerular layer (GL) and (*ii*) to determine the borders of glomeruli that were precisely delimited by the juxtaglomerular zone (Fig. 1*A*). We found that capillaries were exclusively located below the ONL, i.e., in the GL (Fig. 1 *B* and *C*) and in deeper layers (data not shown). To ascertain that capillaries were absent from the ONL, we counted them in two similar volumes (Fig. 1*D*): one cylinder (a 30-μm-thick slice of a glomerulus) located 10–40 μm from the surface of a glomerulus and a second located in the ONL, 10–40 μm above the glomerulus (Fig. 1*D*). In the example shown in Fig. 1, capillaries were absent from the ONL and exclusively present in the three glomeruli (0.3 ± 0.4 and 7 ± 2.7 capillaries per cylinder, respectively). A similar quantification was performed in glomeruli in which we observed the highest density of capillaries (12 animals): capillaries were again exclusively located in the GL (0.3 ± 0.2 and 6 ± 2 capillaries per cylinder in the ONL and GL, respectively). We conclude that, in the olfactory bulb, the presence of capillaries is tightly linked to the sites of synaptic interactions. On the other hand, capillaries often crossed the juxtaglomerular zones linking one glomerulus to its neighbors. This means that, within the GL, the capillary network does not present a differentiation in close relationship with the glomerular organization.

Measurements of the Parameters Characterizing Basal RBC Flow in Individual Capillaries. Intravenous injection of fluorescein dextran revealed the vascular architecture as well as individual RBCs, which appeared as shadows flowing with the fluorescent plasma (Fig. 2*A*). We used rapid line scans (0.5–1 ms) along the capillary axis (10–15 μm) to determine all RBC flow parameters. RBCs moving through the capillary appeared as oblique shadows from which we determined the instantaneous (inst.) RBC flow ($1/T$), velocity (dy/dt), and longitudinal size (velocity.$d\tau$) for each RBC (Fig. 2*B*; see *Methods* for details). Because the tortuosity of capillaries was too important to perform longitudinal line scans over very long distances, the inst.RBC linear density was calculated indirectly as the ratio of inst.RBC flow to inst.RBC velocity. Instantaneous values allowed us to derive power spectra. We observed that inst.RBC flow fluctuated with heartbeats in most capillaries located near arterioles (91%, $n = 11$) but not near venules (Fig. 2*C*). Fluctuations due to respiration were observed in 33% of the animals.

We analyzed basal RBC flow in 43 capillaries. Fig. 3*A* illustrates that the mean value of RBC flow (28 ± 14 RBCs per sec) was correlated to mean values of RBC velocity (0.57 ± 0.28 mm/sec) and RBC linear density (51 ± 12 RBCs per mm) (mean values were calculated as the time average of the instantaneous values over 15–30 sec of data acquisition). Mean RBC velocity and RBC linear density were not found to be correlated ($P \geq 0.1$, Fig. 3*A*, bottom graph). Thus, capillaries with a high mean RBC flow had a high RBC velocity and/or a high RBC linear density. Measurements of instantaneous parameters demonstrated that basal inst.RBC flow is highly variable (Fig. 3*B*). These variations resulted principally from changes in inst.RBC linear density rather than from changes in inst.RBC velocity. In the five capillaries illustrated in Fig. 3*B*, inst.RBC linear density fluctuations (two standard deviations of inst.RBC linear density/mean RBC linear density = 0.65 ± 0.16) were larger than inst.RBC velocity fluctuations (two standard deviations of inst.RBC velocity/mean RBC velocity = 0.26 ± 0.04). In capillaries, the longitudinal size of RBCs was correlated positively to inst.RBC velocity and negatively to inst.RBC linear density ($P < 0.001$ in both cases) (Fig. 3*C*). The increase in RBC longitudinal size with velocity probably results from cell deformation (34) rather than from a change of RBC orientation in the flow. However, RBCs seem to assemble in piles of plates when linear density increases.

Changes in Capillary RBC Flow During Odor Stimulation. At the level of an individual glomerulus, odor stimulation provokes changes in the intensity of intrinsic signals and fMRI signals. These changes partially result from an increase in blood flow. We analyzed inst.RBC flow changes in response to odor stimulation (averages of three to seven odor stimulations) in 27 capillaries from 18 rats. In some cases, several odors were tested, and cases for which none of the tested odors evoked a vascular response

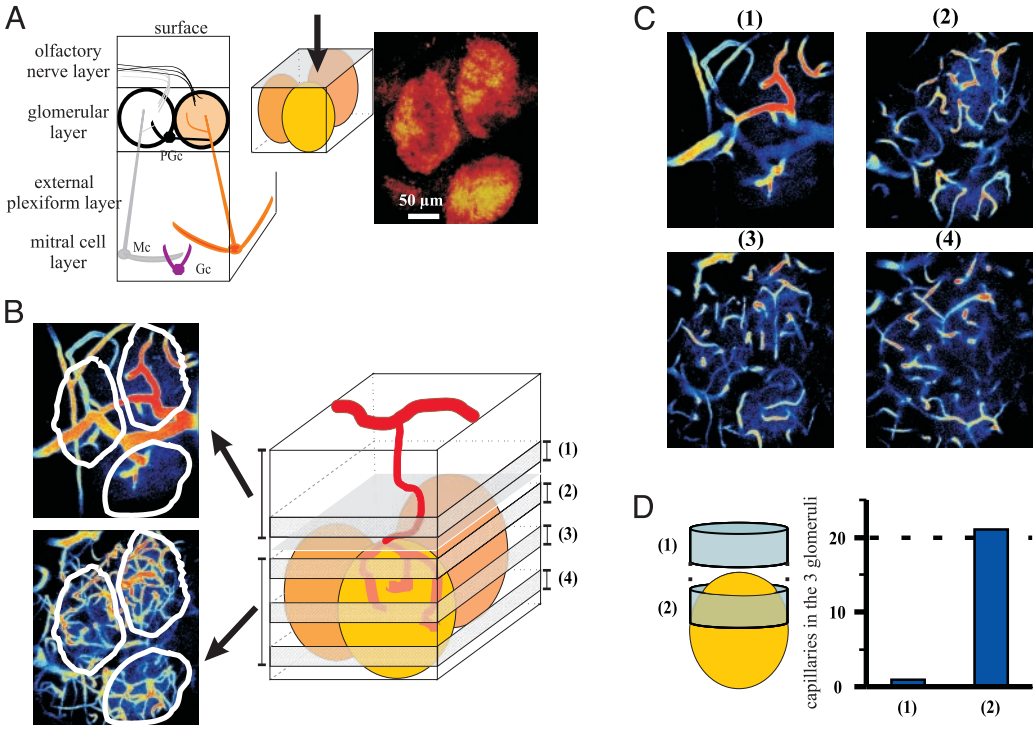

Fig. 1. Vascular architecture of the superficial layers in the rat olfactory bulb. (*A Left*) Schematic representation of the olfactory bulb. Mc, mitral cell; Gc, granule cell; PGc, periglomerular cell. (*A Right*) Three glomeruli labeled with Oregon green dextran (see *Methods*) and imaged by using two-photon microscopy. The image is a two-dimensional projection of 50 images spaced by 2 μm in the *Z* direction (tissue thickness of 100 μm). Note that glomeruli are outlined by the juxtaglomerular zone. (Scale bar, 50 μm.) (*B*) Distribution of vessels in the ONL and GL. Intravenous injection of fluorescein dextran revealed that large vessels run through the ONL, whereas capillaries seem exclusively confined to the GL. The upper image corresponds to a 60-μm stack (30 images) and the lower image corresponds to a 100-μm stack (50 images). The location of the three glomeruli are outlined in white to illustrate that the periglomerular shadows correspond to the juxtaglomerular zone and not to possible light absorption by large superficial vessels. (*C*) Capillaries appear only in the GL, where they invade glomeruli. Four 20-μm stacks (10 images) made above (*1*) and through (*2–4*) the glomeruli, each one spaced 20 μm from the other. Note that capillaries are absent from the first stack (*1*). (*D*) Capillary count in two similar volumes located in and above the three glomeruli.

were discarded. In most cases ($n = 29$), odor caused an increase in inst.RBC flow (23 ± 13%) accompanied by an increase in inst.RBC velocity (23 ± 10%) (Fig. 4). Among these responses, the inst.RBC linear density increased (10 ± 1%) in 5 cases, remained constant in 21 cases, and decreased (12 ± 4%) in 3 cases. Surprisingly, in the remaining 3 cases, RBC flow decreased (25 ± 5%) (Fig. 5*A*). This decrease resulted from a decrease in inst.RBC velocity (16 ± 4%, $n = 3$) accompanied by a decrease in inst.RBC linear density (30 ± 7%, $n = 2$). In all of the cases described above, changes in inst.RBC flow, velocity, and linear density were significant ($P < 0.005$; see *Methods*). Taken together, linear density changed during odor stimulation in 10 of 29 cases. We conclude that neuronal activation can evoke a capillary redistribution of RBCs independently of changes in inst.RBC velocity.

Odor and Glomerular Specificity of Vascular Responses. Axons of sensory cells expressing a precise odorant receptor type converge on one to two glomeruli. As expected, we found that vascular responses of capillaries located in the same glomerulus were similar. Fig. 5*A* illustrates an example where two capillaries responded with similar increases in RBC flow to stimulation with isoamyl acetate. The vascular response was odor-specific because propionic acid induced a decrease in RBC flow in the same capillaries (Fig. 5*A*, bottom graph). Within a glomerulus, we systematically observed that different odorants produce different types of vascular responses.

As mentioned above, the capillary network appeared to be continuous throughout the GL. We therefore investigated how capillaries located in adjacent glomeruli responded to the same odor. We found that capillaries interconnected by the capillary network and separated by only 100–200 μm responded differently to the odor stimulation ($n = 5$). Fig. 5*B* illustrates an extreme case where a high concentration of odor provoked an increase in RBC flow in one glomerulus and no response in the adjacent glomerulus.

During our experiments, animals breathed naturally at ≈2 Hz. Therefore, the onset of neuronal responses fluctuated by ≈0.5 sec. To determine the delay in the vascular response, we first pooled our experiments and observed that RBC velocity apparently increased 1.5–4.2 sec after the onset of odor stimulation (mean delay = 2.5 ± 0.4 sec, $n = 18$). The beginning of the response is defined as the moment when two successive values were larger than twice the noise standard deviation. To determine more precisely the delay between olfactory nerve terminal activation and vascular responses, we placed extracellular recording electrodes in glomeruli in which vascular responses were simultaneously measured. Fig. 5*C* shows a vascular response that lagged behind the beginning of the field potential response by 1.4 sec (mean delay was 1.8 ± 0.2 sec, $n = 7$ animals).

Discussion

In glomerular capillaries, parameters characterizing basal flow, i.e., RBC flow, velocity, and linear density, exhibited large fluctuations over time. Our values are compatible with those reported for capillaries at the cortical surface (for review, see ref. 35) and further in depth when observed with confocal (36, 37) or two-photon laser scanning microscopy (12). In the olfactory bulb, we determined that neither the

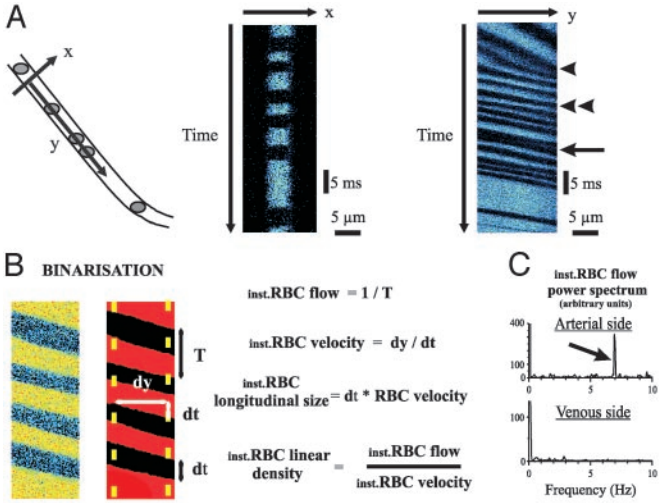

Fig. 2. Technical approaches to measure the parameters of RBC flow in single capillaries. (*A*) Transversal line scans (*X* direction) through capillaries were used to ensure the absence of lateral movements of capillaries as well as to observe RBC flow. Each RBC is seen as a shadow flowing through the fluorescent plasma. Longitudinal line scans (*Y* direction) were used to determine all RBC flow parameters. Note that the slope of oblique shadows and thus RBC velocity could vary (single and double arrowheads) and that occasionally two RBCs were stuck together (arrow). (*B*) Raw data were first binarized (see *Methods*), and values of instantaneous (inst.) flow ($1/T$), velocity (dy/dt), and longitudinal size (velocity.d_T) were determined for each RBC. Inst.RBC linear density was calculated as inst.RBC flow/inst.RBC velocity. Mean values of RBC flow, velocity, or linear density were determined as the time average of the instantaneous values calculated over 20- to 30-sec periods of acquisition. (*C*) Power spectrum analysis of inst.RBC flow reveals that heartbeat fluctuations were essentially observed in capillaries located near arterioles.

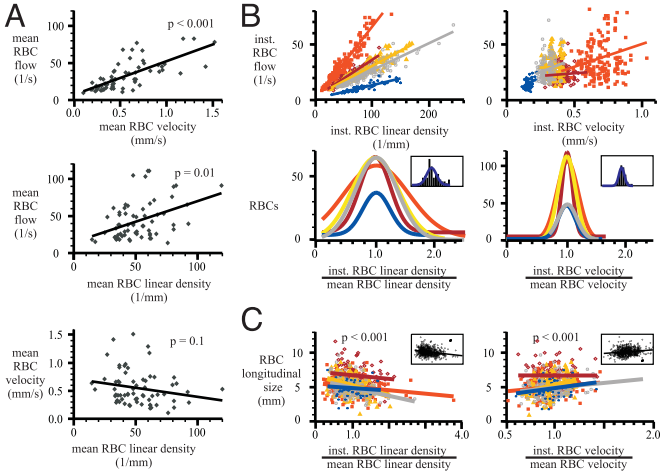

Fig. 3. RBC flow, velocity, linear density, and longitudinal size at rest in glomerular capillaries. (*A*) Mean RBC flow was correlated to mean RBC velocity (*Top*) and to mean RBC linear density (*Middle*). Each dot corresponds to a capillary. Mean RBC velocity varied from 0.1 to 1.6 mm/sec, and mean RBC linear density varied from 14 to 120 RBCs per mm. (*Bottom*) Mean RBC velocity and linear density were independent. (*B*) Variations in inst.RBC flow were principally caused by fluctuations of inst.RBC linear density. *Upper* illustrates that for five capillaries and during a 20- to 30-sec acquisition, the number of RBCs per unit capillary length varied continuously and over a wide range, whereas inst.RBC velocity fluctuated much less. *Bottom* illustrates the extent of these fluctuations. For the five capillaries, the distribution of RBCs as a function of the ratio inst.RBC velocity/mean RBC velocity (*Right*) and the ratio of inst.RBC linear density/mean RBC linear density (*Left*) were plotted with a binning of 0.1 and fitted with a single Gaussian curve. *Insets* show for one capillary (in blue in *Upper*) the superposition of the histograms and the Gaussian curves. Note that velocity varies less than linear density. (*C*) Plots of RBC longitudinal size as a function of inst.RBC linear density/mean linear density (*Left*) and inst.RBC velocity/mean velocity (*Right*). At high linear density, RBCs assembled into piles of plates, whereas at high velocity, RBCs seemed to elongate. *Insets* show the regression lines corresponding to pooled data from the five capillaries. Note that inst.RBC velocity and linear density are independent (data not shown).

mean values nor the instantaneous values of RBC velocity and linear density were correlated. For example, in capillaries with high mean flow and velocity, the mean linear density could be high or low. Moreover, by taking advantage of the possibility to measure these parameters for each individual RBC (i.e., instantaneous values), we observed that the inst.RBC linear density varied continuously, more significantly than and independently of the inst.RBC velocity. The fluctuations of inst.RBC linear density or inst.RBC velocity were too rapid to be related to the 0.1-Hz vasomotion oscillations (38) and were present in conditions of normoxia (see *Methods*). To explain the independence of these two parameters, we hypothesize that a RBC arriving at capillary bifurcation with constant velocity will be directed to one of the two branches according primarily to the branch flow impedance but also to the bifurcation angle and the spatial orientation of the RBC (39).

We used RBC longitudinal size to characterize their orientation and found that the longitudinal size was negatively correlated to the linear density, suggesting that RBCs pile up at high density. More interestingly, RBC longitudinal size also increased with velocity. We attribute this relationship to a deformation of RBCs rather than to a change in orientation. The deformation is probably due to the presence of the endothelial surface layer or glycocalyx. This layer presents a high resistance to flow such that it induces a deformation of RBCs along the axis of flow, in particular when the velocity increases (34, 40). Because velocity increases in response to odor stimulation, we hypothesize that any substance released locally in capillaries adjacent to activated neurons and decreasing the glycocalyx viscosity could decrease the vessel impedance and thus participate in a local capillary regulation of RBC flow.

In 86% of the cases, odor evoked a transient and reproducible increase in RBC flow. This increase was largely due to an increase in RBC velocity. These observations are compatible with neuronal activation inducing an increase in pressure upstream or a decrease in vessel impedance downstream from the recorded capillary. The increase in velocity was accompanied in ≈25% of the cases by a change in RBC linear density. Such functional recruitment (41) of RBCs accompanying the activation of a precise synaptic input has already been described in the cerebellum, by using scanning laser Doppler flowmetry (42). Here, we show that odor stimulation evokes RBC recruitment and "derecruitment" at the level of a single capillary. It is difficult to interpret these observations without a reconstruction of the entire vascular architecture. Indeed, changes in pressure could affect RBC redistribution in branches differently, according to bifurcation angles. Moreover, because some glomeruli are traversed by only one or two capillaries and because the redistribution of RBCs is glomerulus-specific, the redistribution of RBCs should be considered in the interpretation of functional imaging in the olfactory bulb with methods based on the detection of deoxyhemoglobin. In three cases, we observed an odor-evoked decrease in RBC flow. A possible explanation is that odor stimulation drained blood away from the glomerulus in which we were measuring RBC flow to some activated glomeruli. Our experiments in which odor responses were analyzed in two adjacent glomeruli (Fig. 5*B*) did not reveal such blood drainage; however, we cannot exclude this possibility in view of the small number of adjacent glomeruli examined and

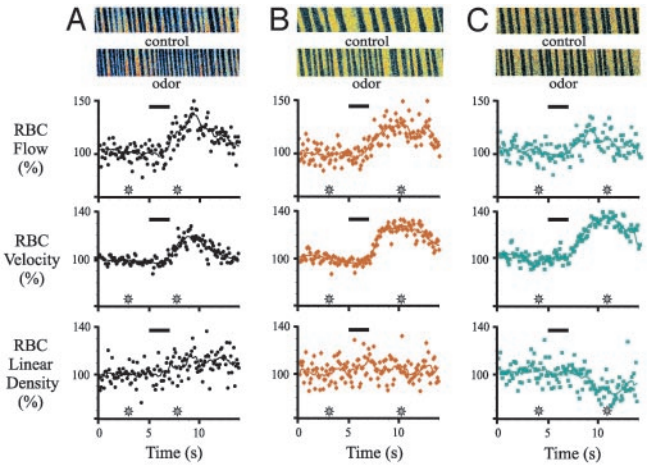

Fig. 4. Isoamyl acetate stimulation evokes various types of RBC flow responses. (*A*) The odor evoked an increase in inst.RBC flow resulting from increases in both velocity and linear density (average of five odor stimulations). (*B*) The odor evoked an increase in inst.RBC flow resulting exclusively from an increase in inst.RBC velocity (average of seven odor stimulations). (*C*) The odor evoked an increase in the inst.RBC flow resulting from a large increase in inst.RBC velocity but accompanied by a decrease in inst.RBC linear density (average of six odor stimulations). Each graph was binned over 100 ms. The continuous line represents the sliding average over 10 bins (1 sec). (*Upper*) Raw data taken at the time indicated by the asterisks in the graphs.

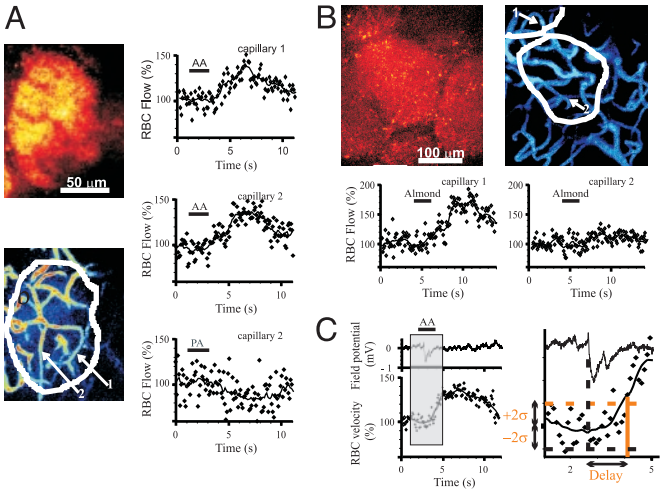

Fig. 5. Properties of odor-evoked vascular responses in a glomerulus. (*A*) Vascular responses in a given glomerulus are odor-specific. A glomerulus was labeled with Oregon green dextran (*Upper Left*), and capillaries were visualized after i.v. injection of fluorescein dextran (*Lower Left*). Isoamyl acetate (AA) induced similar increases in inst.RBC flow in two capillaries (arrows) from the same glomerulus (*Top* and *Middle Right*; average of six and five odor stimulations, respectively). Propionic acid (PA) induced a decrease in inst.RBC flow (*Bottom Right*; average of four odor stimulations). (*B*) Odor-evoked vascular responses are glomerulus-specific. Almond induced a large increase in inst.RBC flow in capillary 1 (arrow), located in an activated glomerulus, but not in capillary 2 (arrow), located in a neighboring glomerulus (average of four and three odor stimulations, respectively). Note that capillaries are interconnected and separated by ≈200 μm. (*C*) Vascular responses occur 1–2 sec after the neuronal response. The vascular response was considered to begin when two successive values exceeded twice the standard deviation of the noise. The field potential electrode and the capillary were located in the same glomerulus. A delay of 1.4 sec separated the electrical and the vascular responses (see the enlargement).

without controlling the vascular responses of all neighboring glomeruli.

To what extent are our results compatible with odor maps obtained with other methods of functional imaging? Two-photon imaging of RBCs demonstrates that RBC flow is correlated to neuronal activity and that vascular capillary responses are glomerular- and odor-specific, observations consistent with those obtained with imaging of calcium (21), voltage (22), and intrinsic signals. Intrinsic signals comprise several parameters involved in blood flow (for review, see ref. 43). Our approach allowed us to determine that both vascular parameters, RBC velocity and linear density, contribute to intrinsic signals. The spatial and temporal resolution of vascular responses imaged with two-photon microscopy is not limited by the technique but rather by the biological response. In particular, the value of RBC linear density and its fluctuations at rest limit the temporal resolution of the technique: it is not possible to investigate what occurs during the first few hundred milliseconds of odor-evoked responses because the number of RBCs moving at a given location in a capillary during this period is too small to discriminate any change in RBC velocity or linear density from noise. Therefore, it is not possible to determine whether a very early change in velocity or linear density occurs coincidentally with what has been referred to as the "initial dip" corresponding to a decrease in deoxyhemoglobin concentration (refs. 44 and 45, but see also refs. 46 and 47). On the other hand, the average delay we observed between odor-evoked neuronal and vascular responses is compatible with that obtained with techniques detecting the inflow of oxygenated blood.

In the bulb, the arteriolar network penetrating into glomeruli from the surface did not exhibit any precise organization that could explain the glomerular specificity of vascular responses to odors. In particular, the few arterioles that branched from descending arteries did not form a network in which each arteriole selectively irrigates a single glomerulus. In addition, the capillary network seemed uniformly distributed within the GL. Thus, the spatial specificity of vascular responses may result from a local capillary regulation, i.e., a change in the glycocalyx viscosity or, most likely, from the organization of venules draining blood from the GL. In the absence of a fluorescent marker specific for venular endothelial cells, two-photon microscopy does not allow for the distinguishing of venules from arterioles and, thus, for reconstruction of the venular network. Such a venular regulation of blood flow could explain the odor responses observed by using BOLD fMRI. Shulman and colleagues (18–20) reported that odors evoke BOLD signals spatially confined to the GL with an extension to the ONL. In the absence of capillaries, the BOLD signal detected in the nerve layer must relate to an increase in deoxyhemoglobin concentration in the veins downstream of activated glomeruli and not to a local increase in metabolism triggered by the activation of olfactory nerve axon bundles. Our hypothesis could depend on the fact that we considered that capillaries had a diameter ≤6 μm. However, when we increased the diameter threshold to 8 μm, the ONL was still mostly devoid of capillaries. Because sensory axons converging on a single glomerulus outnumber principal cells by a factor of several hundred and because action potentials are predicted to consume a major part of the energy budget during signaling (48), our study raises the question of how energy is distributed to olfactory nerve axons, whatever the percentage of them is activated during odor stimulation. Studies based on 2-deoxyglucose consumption (32, 33, 49) clearly demonstrated that energy consumption is significant in the ONL. It is thus possible that the oxygen present in the immediate vicinity of arterioles (50) contributes to the oxygen supply of the ONL. In the absence of a study analyzing the ultrastructure of small vessels in the olfactory bulb superficial layers, the question about the energy distribution to the ONL remains open.

In the rat cerebellar cortex, the groups of Lauritzen (11, 51) and Iadecola (8, 9) have demonstrated that the relationship of presynaptic versus postsynaptic activity with blood flow varies according to the network activated. The determination of the vascular response to odor stimulation at the level of a single capillary allows the step-by-step investigation of the chain of events linking the activation of periglomerular and principal cells to a change in RBC flow.

We thank U. Dirnagl and J. Mertz for their critical comments. This work was supported by the Institut National de la Santé et de la Recherche Médicale, the Ministère de l'Education Nationale de la Recherche et de la Technologie, the Région Ile-de-France (projet Sésame), the Centre National de la Recherche Scientifique, the European Community (5th Programme Cadre de Recherche et Developpement de la Commission Européene; QLG3-CT-2000-00934), the Fondation pour la Recherche Médicale (ICP20001222128), and the Humboldt Foundation. E.C. is supported by a fellowship from the Direction Générale de l'Armement.

1. Villringer, A. & Dirnagl, U. (1995) *Cerebrovasc. Brain Metab. Rev.* **7,** 240–276.
2. Magistretti, P. J., Pellerin, L., Rothman, D. L. & Shulman, R. G. (1999) *Science* **283,** 496–497.
3. Attwell, D. & Iadecola, C. (2002) *Trends Neurosci.* **25,** 621–625.
4. Logothetis, N. K., Pauls, J., Augath, M., Trinath, T. & Oeltermann, A. (2001) *Nature* **412,** 150–157.
5. Smith, A. J., Blumenfeld, H., Behar, K. L., Rothman, D. L., Shulman, R. G. & Hyder, F. (2002) *Proc. Natl. Acad. Sci. USA* **99,** 10765–10770.
6. Raichle, M. E. & Gusnard, D. A. (2002) *Proc. Natl. Acad. Sci. USA* **99,** 10237–10239.
7. Logothetis, N. K. (2003) *J. Neurosci.* **23,** 3963–3971.
8. Iadecola, C., Li, J., Xu, S. & Yang, G. (1996) *J. Neurophysiol.* **75,** 940–950.
9. Yang, G. & Iadecola, C. (1998) *Stroke* **29,** 499–507.
10. Mathiesen, C., Caesar, K., Akgoren, N. & Lauritzen, M. (1998) *J. Physiol. (London)* **512,** 555–566.
11. Lauritzen, M. & Gold, L. (2003) *J. Neurosci.* **23,** 3972–3980.
12. Kleinfeld, D., Mitra, P. P., Helmchen, F. & Denk, W. (1998) *Proc. Natl. Acad. Sci. USA* **95,** 15741–15746.
13. Svoboda, K., Denk, W., Kleinfeld, D. & Tank, D. W. (1997) *Nature* **385,** 161–165.
14. Charpak, S., Mertz, J., Beaurepaire, E., Moreaux, L. & Delaney, K. (2001) *Proc. Natl. Acad. Sci. USA* **98,** 1230–1234.
15. Shepherd, G. M. & Greer, C. A. (1998) in *The Synaptic Organization of the Brain*, ed. Shepherd, G. M. (Oxford Univ. Press, New York), pp. 159–203.
16. Vassar, R., Chao, S. K., Sitcheran, R., Nunez, J. M., Vosshall, L. B. & Axel, R. (1994) *Cell* **79,** 981–991.
17. Ressler, K. J., Sullivan, S. L. & Buck, L. B. (1994) *Cell* **79,** 1245–1255.
18. Yang, X., Renken, R., Hyder, F., Siddeek, M., Greer, C. A., Shepherd, G. M. & Shulman, R. G. (1998) *Proc. Natl. Acad. Sci. USA* **95,** 7715–7720.
19. Xu, F., Kida, I., Hyder, F. & Shulman, R. G. (2000) *Proc. Natl. Acad. Sci. USA* **97,** 10601–10606.
20. Kida, I., Xu, F., Shulman, R. G. & Hyder, F. (2002) *Magn. Reson. Med.* **48,** 570–576.
21. Wachowiak, M. & Cohen, L. B. (2001) *Neuron* **32,** 723–735.
22. Spors, H. & Grinvald, A. (2002) *Neuron* **34,** 301–315.
23. Rubin, B. D. & Katz, L. C. (1999) *Neuron* **23,** 499–511.
24. Uchida, N., Takahashi, Y. K., Tanifuji, M. & Mori, K. (2000) *Nat. Neurosci.* **3,** 1035–1043.
25. Belluscio, L. & Katz, L. C. (2001) *J. Neurosci.* **21,** 2113–2122.
26. Luo, M. & Katz, L. C. (2001) *Neuron* **32,** 1165–1179.
27. Meister, M. & Bonhoeffer, T. (2001) *J. Neurosci.* **21,** 1351–1360.
28. Yuan, Q., Harley, C. W., McLean, J. H. & Knopfel, T. (2002) *J. Neurophysiol.* **87,** 3156–3159.
29. Imamura, K., Mataga, N. & Mori, K. (1992) *J. Neurophysiol.* **68,** 1986–2002.
30. Katoh, K., Koshimoto, H., Tani, A. & Mori, K. (1993) *J. Neurophysiol.* **70,** 2161–2175.
31. Yokoi, M., Mori, K. & Nakanishi, S. (1995) *Proc. Natl. Acad. Sci. USA* **92,** 3371–3375.
32. Stewart, W. B., Kauer, J. S. & Shepherd, G. M. (1979) *J. Comp. Neurol.* **185,** 715–734.
33. Johnson, B. A., Woo, C. C. & Leon, M. (1998) *J. Comp Neurol.* **393,** 457–471.
34. Secomb, T. W., Hsu, R. & Pries, A. R. (2001) *Am. J. Physiol.* **281,** H629–H636.
35. Hudetz, A. G. (1997) *Microcirculation.* **4,** 233–252.
36. Villringer, A., Them, A., Lindauer, U., Einhaupl, K. & Dirnagl, U. (1994) *Circ. Res.* **75,** 55–62.
37. Seylaz, J., Charbonne, R., Nanri, K., Von Euw, D., Borredon, J., Kacem, K., Meric, P. & Pinard, E. (1999) *J. Cereb. Blood Flow Metab.* **19,** 863–870.
38. Mayhew, J. E., Askew, S., Zheng, Y., Porrill, J., Westby, G. W., Redgrave, P., Rector, D. M. & Harper, R. M. (1996) *NeuroImage* **4,** 183–193.
39. Pries, A. R., Secomb, T. W. & Gaehtgens, P. (1996) *Cardiovasc. Res.* **32,** 654–667.
40. Vink, H. & Duling, B. R. (1996) *Circ. Res.* **79,** 581–589.
41. Kuschinsky, W. & Paulson, O. B. (1992) *Cerebrovasc. Brain Metab. Rev.* **4,** 261–286.
42. Akgoren, N. & Lauritzen, M. (1999) *NeuroReport* **10,** 3257–3263.
43. Grinvald, A., Shmuel, A., Vanzetta, I., Shoham, D. & Arieli, A. (2000) in *Imaging Neurons*, eds. Yuste, R., Lanni, F. & Konnerth, A. (Cold Spring Harbor Lab. Press, Plainview, NY), pp. 45.1–45.17.
44. Malonek, D. & Grinvald, A. (1996) *Science* **272,** 551–554.
45. Vanzetta, I. & Grinvald, A. (1999) *Science* **286**, 1555–1558.
46. Vanzetta, I. & Grinvald, A. (2001) *NeuroImage* **13,** 959–967.
47. Lindauer, U., Royl, G., Leithner, C., Kuhl, M., Gold, L., Gethmann, J., Kohl-Bareis, M., Villringer, A. & Dirnagl, U. (2001) *NeuroImage* **13,** 988–1001.
48. Attwell, D. & Laughlin, S. B. (2001) *J. Cereb. Blood Flow Metab.* **21,** 1133–1145.
49. Sharp, F. R., Kauer, J. S. & Shepherd, G. M. (1975) *Brain Res.* **98,** 596–600.
50. Tsai, A. G., Friesenecker, B., Mazzoni, M. C., Kerger, H., Buerk, D. G., Johnson, P. C. & Intaglietta, M. (1998) *Proc. Natl. Acad. Sci. USA* **95,** 6590–6595.
51. Lauritzen, M. (2001) *J. Cereb. Blood Flow Metab.* **21,** 1367–1383.